HHS Public Access

Author manuscript

J Am Chem Soc. Author manuscript; available in PMC 2020 March 06.

Published in final edited form as:

J Am Chem Soc. 2019 March 06; 141(9): 3863–3874. doi:10.1021/jacs.8b08421.

Spin-Dependent Ionization of Chiral Molecular Films

John M. Abendroth[1,2], **Kevin M. Cheung**[1,2], **Dominik M. Stemer**[1,3], **Mohammed S. El Hadri**[4], **Chuanzhen Zhao**[1,2], **Eric E. Fullerton**[4], **Paul S. Weiss**[1,2,3,*]

[1]California NanoSystems Institute, University of California, Los Angeles, Los Angeles, CA 90095, United States

[2]Department of Chemistry & Biochemistry, University of California, Los Angeles, Los Angeles, CA 90095, United States

[3]Department of Materials Science & Engineering, University of California, Los Angeles, Los Angeles, CA 90095, United States

[4]Center for Memory and Recording Research, University of California, San Diego, La Jolla, CA 92093, United States

Abstract

Spin selectivity in photoemission from ferromagnetic substrates functionalized with chiral organic films was analyzed by ultraviolet photoelectron spectroscopy at room temperature. Using radiation with photon energy greater than the ionization potential of the adsorbed molecules, photoelectrons were collected that originated from both underlying ferromagnetic substrates and the organic films, with kinetic energies in the range of *ca.* 0–18 eV. We investigated chiral organic films composed of self-assembled monolayers of α-helical peptides and electrostatically adsorbed films of the protein, bovine serum albumin, with different α-helix and β-sheet content. Ultraviolet photoelectron spectral widths were found to depend on substrate magnetization orientation and polarization, which we attribute to helicity-dependent molecular ionization cross sections by photoelectron impact, possibly resulting in spin-polarized holes. These interactions between spin-polarized photoelectrons and chiral molecules are physically manifested as differences in the measured photoionization energies of the chiral molecular films. Substrate magnetization-dependent ionization energies and work function values were deconvoluted using surface charge neutralization techniques, permitting the measurement of relative spin-dependent energy barriers to transmission through chiral organic films.

graphical abstract

*Corresponding author: psw@cnsi.ucla.edu (PSW).

ASSOCIATED CONTENT

Supporting Information

Supporting Information is available free of charge on the ACS Publication website at DOI:. Materials and experimental methods are provided, as well as additional data used to evaluate the conclusions in the paper. Figures, tables, and experimental details describe the analysis of ultraviolet photoelectron spectra; elemental analysis of the molecular films using X-ray photoelectron spectroscopy; characterization of peptides and proteins by circular dichroism spectroscopy; characterization of peptides and proteins on surfaces *via* infrared reflection-absorption spectroscopy, ellipsometry, and atomic force microscopy; UPS control measurements; and statistical analysis.

The authors declare no competing financial interest.

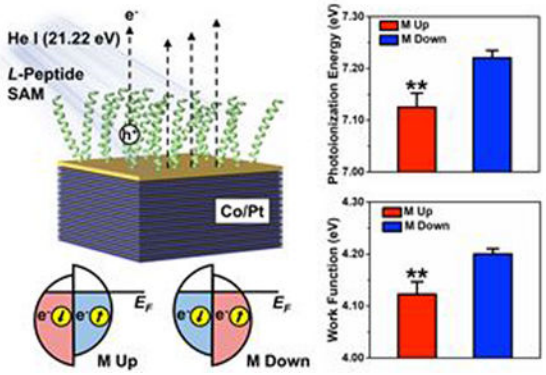

Keywords

chiral-induced spin selectivity (CISS) effect; spin-polarized electrons; ferromagnet; bovine serum albumin; ionization potential; work function modulation

INTRODUCTION

Enantioselective interactions between chiral molecules and electrons that depend on electron helicity, that is, the projection of an electron's spin angular momentum on its linear momentum, enable the generation and manipulation of spin-polarized electrons at room temperature.[1,2] This spin-filtering phenomenon is attributed to the chiral-induced spin selectivity (CISS) effect,[3–5] analogous to electron dichroism by gas-phase chiral molecules,[6,7] and has attracted recent attention in studying charge transfer[8–13] and polarization[14–17] over a wide range of dissymmetric molecular systems. Spin polarization in photoelectron transmission through chiral organic monolayers has been measured explicitly, using both linearly and circularly polarized radiation to emit unpolarized or longitudinally polarized photoelectrons, respectively, from noble metal substrates.[18–21] In these studies, photon energies lower than the ionization potentials of the adsorbed organic films were used to excite photoelectrons solely from the underlying metal surfaces. However, little is known about the relative energetic barriers to transmission of spin-up vs spin-down electrons through chiral organic films within this charge transport regime, or how the use of ionizing radiation may influence spin-dependent photoemission from chiral molecular films.

Herein, using ultraviolet photoelectron spectroscopy (UPS), we characterized the valence electronic structure of ferromagnetic multilayer (FM) surfaces with adsorbed chiral molecules as a function of molecular chirality and secondary structure, substrate magnetization orientation, average substrate polarization magnitude, and photoemission angle. Using unpolarized ionizing radiation from a helium-ion ultraviolet light source (He I emission line), we collected primary and secondary valence photoelectrons that originated from both the FM substrates and adsorbed chiral molecule films composed of α-helical peptides, or proteins with varying α-helix and β-sheet content. Our experiments were designed to deconvolute potential mechanisms of room-temperature spin filtering in photoemission by ionizing radiation, and to measure the relative energy barriers to over-the-barrier transmission of spin-up *vs* spin-down electrons through chiral molecular assemblies.

The experimental schematic for the UPS measurements is illustrated in Figure 1. Spin selectivity in photoemission from FM substrates functionalized with chiral organic films may be attributed to the following possible processes. Nominally, the spin polarization of photoelectrons from FM substrates reflects the polarization within the material itself; an incident photon excites an electron below the Fermi level to a final state with identical spin.[22,23] However, when FM substrates are functionalized with chiral films, the spin polarization of photoelectrons emitted from the metal depends on the chirality of the adsorbed molecules that act as spin filters. Spin filtering is due to the asymmetric scattering probabilities of electrons with opposite helicity, and spatial structure of unoccupied high-lying states.[18–21,24] Compared to randomly dispersed molecules in the gas phase, surface assemblies impart orientation and alignment that enhances and focuses asymmetry in scattering of low kinetic energy electrons. The higher density of molecules within a film compared to that within the gas phase enables the interaction of photoelectrons with strengthened chiral fields due to proximity effects.[24]

The work function (ϕ), defined as the difference between the photon energy, $h\nu$ (21.22 eV), and the binding energy of the secondary electron cutoff (*i.e.*, maximum binding energy), E_B^{max}:

$$\phi = h\,\nu\, - E_B^{max} \quad (1)$$

of FM surfaces should depend on both the magnetization orientation of the FM substrate, and on the molecular handedness. This value represents the energy barrier to remove an electron from the solid surface to a point in the vacuum infinitely far from the surface. Thus, when the spin state of majority-spin electrons match the preferred spin orientation of electrons transmitted through chiral monolayers, a lower ϕ is expected.

If the photon energy is higher than the ionization potential of the organic film, such as in UPS measurements, electrons are also collected from occupied electronic states within the organic films by ionizing the adsorbed molecules. Spin-polarized photoemission by ionization of surface adsorbates has been detected using circularly polarized light, which is solely a result of spin-orbit interactions that depends on the helicity of the incident photons, and is therefore more prominent in high-Z systems.[25] Photoemission from diamagnetic molecules using unpolarized or linearly polarized radiation, however, is not expected to yield spin-polarized photoelectrons.[26]

Still, ionization of chiral molecules by impact of photoelectrons with sufficient energy that originate from the metal surface may be electron helicity dependent. Ionizing collisions between spin-polarized electrons and atomic targets show helicity-dependent cross sections resulting from electron exchange and angular-momentum coupling, even for non-relativistic (small spin-orbit coupling) models.[27,28] Moreover, scattering of secondary electrons within a chiral film that leads to spin polarization may leave behind an excess of holes of a particular spin state upon ionization, dictated by the handedness of the organic material and/or helicity of the scattering electron.

The photoionization energy of the organic film (I) is defined as the energy difference between the photon energy and the width of the photoelectron spectra:

$$I = h\nu - \left(E_B^{max} - E_B^{min}\right) = h\nu - W \quad (2)$$

where E_B^{min} and W represent the valence band edge (*i.e.*, minimum binding energy) and the spectral width, respectively. An electron-helicity-dependent ionization cross section would be physically manifested as a dependence of I on substrate magnetization orientation, resulting from a different buildup of positive charges in an organic layer for FM substrates magnetized up *vs* down. Note that ensemble photoionization potentials of the films would then be oppositely related to the propensity of electron helicity- and chirality-dependent molecular ionization by electron impact. Additionally, if the holes within the chiral organic films are spin polarized, they must be filled by electrons with a matching spin state supplied from the grounded FM substrate.[29] In this case, holes would be more efficiently filled when substrates are in the preferred magnetization orientation, corresponding to a lower I. In the opposite magnetization orientation, a greater accumulation of positive charge within the chiral organic layer would result in a higher I.

Finally, spin polarization may occur solely *via* electron transfer by conduction from the underlying metal to neutralize the buildup of positive charge within organic films during measurements with a dependence on the handedness of the organic layer. The CISS effect has been demonstrated within this charge-transfer regime for bound electrons,[11,12] and spin-valve-like architectures between FM layers and chiral molecules show high- or low-resistance states dictated by the substrate magnetization orientation and molecule chirality.[8,9,13,20] Thus, differences in I between substrate magnetization orientations may result from spin-dependent charge transfer through the chiral organic molecules.

RESULTS

Ferromagnetic Substrate Characterization.

Ferromagnetic substrates with perpendicular magnetic anisotropy were grown on glass substrates with a composition of Ta 3/Pt 2/[Co 0.6/Pt 0.3]$_{69}$/Co 0.6/Au 1 (layers in nm) and used for UPS measurements. While the thin layer of Au is insufficient to prevent partial oxidation of the first underlying Co layer(s) (Figure S1), it enables the formation of stable molecular films of thiolated molecules due to the formation of robust Au-S bonds, while also maintaining the polarization of electrons originating from the Co layers.[9,13]

The magnetic hysteresis of this substrate material is shown in Figure 2a. The substrates retain their magnetization out of the plane of the films upon removal of external magnetic fields. Substrates were designed with large coercivities (~3 kOe) to prevent loss of initial magnetization within the instrument chamber due to magnetic fields used to focus photoelectrons to the detector. As indicated by the slanted shape of the hysteresis curves due to the large substrate coercivity, our substrate design also made it possible to magnetize substrates reproducibly to sub-saturation conditions *via* minor loops (as shown by the open

symbols in Figure 2a). We investigated conditions for UPS measurements when the substrates were magnetized with a saturating field of ±12 kOe and reverse field of ±7 kOe after saturation to probe different average spin polarizations (*i.e.*, ratio of spin-up to spin-down electrons) within the FM substrate.

Complete representative ultraviolet photoelectron spectra, and enlarged regions of the secondary electron cutoff and Fermi edge for bare substrates are shown in Figure 2b and 2c at full saturation, respectively. No differences in ϕ were measured between opposite magnetization conditions for bare substrates (Figure 2d). Importantly, these results show that the influence of remnant magnetic fields at the surface of the perpendicularly magnetized substrates (attributed to surface roughness) at saturation on emitted photoelectrons is negligible. Additionally, no significant differences were found in the secondary electron peak intensities nor total integrated areas of the spectra between substrate magnetization conditions (Table S1). The energies of the secondary electron cutoffs, Fermi edges, and ϕ can be found in Table S2.

Spin-Selective Photoemission from *L*-Peptide Monolayers.

We investigated right-handed α-helical peptides (henceforth *L*-peptides) composed of (N terminus → C terminus) $[K(Aib)A(Aib)A]_6KC$, where K, A, and C represent the amino acid residues lysine, alanine, and cysteine, respectively. The achiral 2-aminoisobutyric acid (Aib) residues were used to stabilize the α-helical secondary structure of the peptides,[10] which was confirmed in solution by circular dichroism spectroscopy (Figure S2). Self-assembled monolayers (SAMs) of *L*-peptides were formed on FM substrates by binding of the thiol functional group of cysteine residues on the C-termini of the oligopeptides to the Au capping layers (Figure 3a). Peptide assembly on FM surfaces was confirmed by the presence of amide I and II stretching bands observed *via* infrared reflection-absorption spectroscopy (Figure S3a).

Full representative ultraviolet photoelectron spectra and enlarged regions of the secondary electron cutoff and valence band edges of *L*-peptide SAMs are shown in Figures 3b and 3c, respectively. The average energies of E_B^{min} and E_B^{max} measured for each magnetization condition are shown in Figure 3d.

Two-way analysis of variance showed a significant interaction between substrate magnetization orientation and saturation condition for I when FM substrates were functionalized with *L*-peptide SAMs. *Post hoc* analysis revealed that ionization energies were significantly *lower* when the magnetization of substrates were oriented up *vs* down only when FM substrates were fully magnetized (Figure 3e, $^{**}P < 0.01$). When the spin polarization of the substrate was lowered by magnetizing the samples with a sub-saturating field, no significant differences between magnetization orientations were found. These data indicate that both the magnetization orientation and the magnitude of the average spin polarization of the substrate influenced the measured ionization energies for *L*-peptide SAMs on FM substrates.

The negative shift in ϕ of the substrates upon *L*-peptide functionalization indicates covalent binding of the thiolated cysteine residues to the metal surface due to the positive dipole (C terminus → N terminus) of the α-helices pointing away from the surfaces (Table S2).[30–32] However, no significant differences in ϕ were determined between magnetization orientations at saturation. Furthermore, no significant differences in secondary electron peak intensities nor total integrated areas of the spectra were determined between substrate magnetization orientations under either full or sub-saturation conditions (Table S2).

Because our laboratory axis of electron spin polarization within the FM substrates is defined as the surface normal (up *vs* down), and because spin polarization by the CISS effect is expected to be along the axis of helical molecules,[33–40] we hypothesize that molecular orientation influences the observed dependence of ionization energy on substrate magnetization. The alignment of the *L*-peptides was determined by measuring the thicknesses of SAMs on FM surfaces by ellipsometry (Table S3). The average thickness of *L*-peptide SAMs was 3.7 ± 0.5 nm. Assuming a rise of 0.15 nm per amino acid residue, the length of a peptide of 32 resides would be 4.8 nm. Thus, the measured thickness may be a result of off-normal orientation (*ca.* 40° relative to the surface normal) of the *L*-peptide molecules within the SAMs, or incomplete coverage due to the surface roughness induced in film growth to increase substrate coercivity (Figure S4).

We also tested for dependence of *I* on the substrate magnetization orientation when collecting photoelectrons at angles of 15° and 30° relative to the surface normal by tilting the samples (Figure 3f). While peak intensities and integrated areas decreased with increasing angle of photoemission (Figure S5), differences between substrate magnetization conditions remained insignificant. Two-way analysis of variance showed *no* significant interaction between substrate magnetization orientation and collection angle (0°, 15°, and 30° relative to the surface normal) for *I*. This finding indicates that *I* does not depend on *both* magnetization orientation and angle. However, *post hoc* analysis revealed that ionization energies were significantly *lower* when the magnetization of substrates were oriented up *vs* down at all three angles ($^*P < 0.05$). These results suggest that the relative differences in *I* are indirectly related to spin-selective effects in photoelectron interaction with the chiral films (*vide infra*).

Notably, all peptide SAMs were assembled after clean FM substrates were first magnetized up or down. Spin-specific interactions have been shown to occur upon adsorption and charge transfer when chiral molecules bind to ferromagnetic substrates, resulting in magnetization induced by the proximity of adsorbed chiral molecules.[15] Recently these surface-charge-mediated interactions enabled the enantiomeric separation of racemic mixtures by achiral ferromagnetic substrates.[16] The rates of adsorption of one enantiomer *vs* the other on substrates magnetized up *vs* down were different, even though binding energies are identical. Thus, preferential adsorption of one enantiomer over another based on substrate magnetization was hypothesized to occur on short time scales (on the order of seconds).[16] These transient interactions may be analogous to long-range substrate-mediated intermolecular interactions that govern molecular ordering and alignment, such as in the nascent stages of SAM formation, surface catalysis, and nanostructure formation.[41,42] Molecular films move towards (although never reach) thermodynamic equilibrium during

SAM formation,[41,43–45] which likely explains the reduced enantioselectivity in adsorption observed by Banerjee-Ghosh *et al.* at longer time scales.[16]

Herein, SAMs were formed over 48 h, so differences in SAM stabilities or densities between substrate magnetization orientations for the same enantiomer should be negligible. We compared C 1s regions of X-ray photoelectron spectra collected from *L*-peptide SAMs to test if the density of *L*-peptides on the surfaces depended on the initial magnetization of the substrates (Figure S6a). We found that there was *no* significant difference in the total integrated areas of the C 1s peaks between substrates initially magnetized up *vs* down, suggesting negligible dependence of *L*-peptide film formation on substrate magnetization after 48 h of incubation (Figure S6b). Further, we measured *I* when substrates were *post*-magnetized to the opposite orientation following SAM formation, and reproduced our results from testing *L*-peptide films on *pre*-magnetized-only samples (Figure 3e), measuring a lower ionization energy when substrates were *post*-magnetized up *vs* down (Figure S7).

Based on results observed with *L*-peptide SAMs, we hypothesized that surfaces functionalized with *D*-peptide SAMs of opposite chirality (Figure S8), where each K, A, and C residues are of *D*-form, would show instead *higher I* when the magnetization of substrates were oriented parallel to the surface normal. Preparation of SAMs and UPS measurements (Figure S9) were performed in identical manners to those of *L*-peptide films. However, two-way analysis of variance showed no significant interaction between substrate magnetization orientation and saturation condition, nor significance in the main effects for *I* when FM substrates were functionalized with *D*-peptide SAMs.

We posit that the absence of any dependence of *I* on the substrate magnetization may be due to poorer SAM quality of *D*-peptides *vs L*-peptides. Despite appearing nearly indistinguishable by atomic force microscopy (Figure S10), the average thickness of *D*-peptide SAMs was 1.9 ± 0.3 nm (Table S3), suggesting an even poorer surface coverage or greater tilt (*ca.* 67° relative to the surface normal) compared to that of *L*-peptide SAMs. These results reflect the lower signal intensity measured in infrared reflection-absorption measurements (Figure S3). Deviation of molecules from alignment normal to the surface should result in lower spin-filtering efficiency. Further, higher densities of chiral molecules are expected to yield larger spin polarization in electron transmission due to wavefunction overlap with multiple molecules.[24,46] Thus, we attribute the absence of substrate magnetization dependence of the ionization potential of *D*-peptide SAMs to low surface coverage.

We also tested mixed SAMs composed of *L*- and *D*-peptides formed from racemic mixtures. While SAMs formed from racemic mixtures may result in phase separation into homochiral conglomerates,[42,47] because each photoelectron spectrum represents an ensemble characterization of the surfaces, dilution of *L*-peptide SAMs with molecules of the opposite chirality in this manner was hypothesized to result in no net measurable spin selectivity in photoemission. Indeed, there were no observable differences in *I* between substrate magnetization orientations when fully saturated (Figure S11). These results agree qualitatively with the seminal work done by Ray *et al.*, who observed that enantioselectivity in the transmission of spin-polarized photoelectrons emitted from Au using left- *vs* right-

handed circularly polarized light through films of *L*-stearoyl lysine films disappeared when films were formed with minor (1%) impurities of *D*-stearoyl lysine.[24]

Spin-Selective Photoemission from Protein Films.

To investigate the influence of structure and orientation on spin-selective photoemission, ultraviolet photoelectron spectra were also compared between FM substrate magnetization conditions when surfaces were functionalized with adsorbed films of the protein, bovine serum albumin (BSA), in unmodified *vs* thermally denatured (dBSA) conditions (Figure 4a). Adsorption of BSA on various surfaces has been widely investigated, and generally, higher densities are achieved using charged substrates compared to hydrophobic surfaces.[48,49] Thus, positively charged SAMs of achiral 11-amino-1-undecanethiolate (AUT) monolayers were formed first on FM substrates (Figure S12) to facilitate the electrostatic binding of BSA molecules by association with negatively charged residues on the proteins.[50]

In its native conformation, the globular protein, BSA, is composed of multiple right-handed α-helical subunits with *ca.* 60% structural helicity. However, upon adsorption on surfaces and dehydration, conditions necessary for the experiments performed herein, pristine secondary structure is lost, with a decrease in structural helicity and slight increase in β-sheet content.[51,52] When irreversibly denatured due to heating prior to surface assembly, greater loss of structural helicity and conversion to conformations with higher composition of β-sheets is evident by circular dichroism spectroscopy (Figure S13).[53] Infrared reflection-absorption spectroscopy confirms the greater β-sheet content of dBSA when dried on FM substrates based on analysis of the amide I band with reduction of absorbance in the range 1655–1650 cm^{-1}, attributed to α-helical composition, and increase in absorbance in the range 1685–1633 cm^{-1}, due to β-sheets (Figure S14).[54] Still, the chemical nature of the protein is not lost by thermal denaturation as evidenced by comparison of the nearly identical C 1s, N 1s, and O 1s regions of high-resolution X-ray photoelectron spectra for BSA and dBSA films on AUT SAMs (Figure S15). Thus, films composed of dBSA have reduced α-helicity, but maintain chirality due to the *L*-amino acid subunits within the reorganized proteins.

The energies of the secondary electron cutoffs and valence band edges of ultraviolet photoelectron spectra obtained from FM substrates functionalized with AUT SAMs and BSA or dBSA films at full- and sub-saturation magnetization conditions (Figure S16) are shown in Figure 4b. Similar to the measurements of *L*- and *D*-peptide SAMs, no significant differences in secondary electron peak intensities, total integrated area of the spectra, or ϕ were determined between substrate magnetization orientations for each condition (Tables S1,2).

Two-way analysis of variance showed no significant interaction between substrate magnetization orientation and saturation condition, nor significance in the main effects for *I* when FM substrates were functionalized with BSA films (Figure 4c). We attribute the absence of the dependence of spectral widths on magnetization condition to the random orientation of disordered α-helical subunits and overall lower α-helical content that occurs upon surface adsorption, as indicated by infrared reflection-absorbance spectroscopy, compared to that of well-aligned *L*-peptide SAMs.

Alternatively, two-way analysis of variance showed significant interactions between substrate magnetization orientation and saturation conditions for I when FM substrates were functionalized with AUT SAMs and dBSA films (Figure 4d). *Post hoc* analysis showed that values of I were significantly *higher* when the magnetization of substrates were oriented up *vs* down only when FM substrates were fully magnetized ($^{*}P < 0.05$). Again, when the spin polarization of the substrate was lowered by magnetizing the samples with a sub-saturating field, no significant differences between magnetization orientations were found.

No differences in I were measured between opposite magnetization orientations of FM substrates at full saturation when functionalized with achiral AUT SAMs only (Figure S17). These results are expected, as no dependence of transmission on electron helicity should occur if the molecular films are achiral, and provide additional evidence that the observations for *L*-peptide SAMs and AUT SAMs with dBSA films are not artifacts attributed to magnetic fields at the metal surfaces of the FM substrates due to remnant magnetization of the substrates.

Photoemission Measurements with Surface Charge Neutralization.

The grounded, conductive FM substrates provide a source of (spin-polarized) electrons to fill holes within the ionized chiral films during measurement. Still, with the exception of bare FM samples, positive charging of the surfaces under all conditions was evident by a shift in ultraviolet photoelectron spectra to higher binding energies upon multiple scans on the same substrates (Figure S18). To test if magnetization-dependent differences in the photoelectron spectral features were due to differences in positive charging within the films upon photoelectron-induced ionization, nondestructive (Figure S19) charge neutralization methods were employed to minimize charging attributed to this possibility.[55,56]

On average, for FM substrates functionalized with *L*-peptide SAMs, lower values of I were measured with charge neutralization when compared to the aforementioned measurements without use of the electron flood gun, indicative of a reduction in the positive charging of the organic films by this method (Table S2). Using the electron flood gun, no significant differences in I as a function of magnetization orientation were determined at full magnetization saturation (Figure 5a). These results confirm that positive charging, and thus, photoionization energies, of *L*-peptide SAMs upon ionization depend on substrate magnetization orientation.

In addition, differences in ϕ were observed with charge neutralization between magnetization orientations as indicated by different shifts in the secondary electron cutoff positions (Figure 5b). A lower ϕ was measured for FM surfaces functionalized with *L*-peptide SAMs when substrates were magnetized up (Figure 5c). We hypothesize that shifts in ϕ became apparent by deconvoluting the influence of substrate magnetization-dependent charging of the ionized chiral organic films on the photoelectron spectra.

We also tested the influence of charge neutralization on I and ϕ for AUT SAMs with dBSA films on fully saturated FM substrates between substrate magnetization orientations. Again, a decrease in I was observed compared to measurements without use of the electron flood

gun, and no differences between magnetization up *vs* down conditions were determined (Figure 5d), analogous to measurements with *L*-peptide SAMs. However, no substrate magnetization-dependent differences in ϕ were observed with charge neutralization for AUT SAMs with dBSA films (Figure 5e,f). We attribute these results to the larger thicknesses of AUT SAMs with dBSA films (9.4 ± 0.4 nm) compared to *L*-peptide SAMs, as indicated by ellipsometry measurements (Table S3). The thicker organic layers may attenuate transmission of photoelectrons originating from the FM substrate sufficiently to prevent resolution of ϕ differences in our measurements. Further, characterization of AUT SAMs with adsorbed BSA and dBSA films by atomic force microscopy indicate greater surface inhomogeneity compared to bare FM substrates, *L*- or *D*-peptide SAMs, or AUT SAMs (Figure S20), which may also mask subtle differences in ϕ.

Finally, while electrons from the flood gun are initially unpolarized, we cannot rule out the possibility that the chiral molecules polarize these electrons. It is unclear if the relative polarization of electrons in the majority and minority spin subbands of the FM substrates would then influence charge neutralization of the adsorbed molecules, and thus requires further investigation.

Testing Spin-Dependent Conduction through Protein Films.

The aforementioned differences in *I* may also be due to more efficient transfer of spin-polarized conduction electrons supplied by the underlying metal surface to neutralize the chiral layers under one magnetization orientation *vs* the opposite. Electron-helicity-dependent charge transfer through *L*- and *D*-peptides has been reported previously, and is not tested here.[57,58] To test if BSA or dBSA films can effectively filter electrons transferred in the tunneling/hopping regime as well, solid-state spin-valve devices were fabricated to measure spin selectivity in conduction. Non-ferromagnetic Au electrodes, functionalized with AUT SAMs and BSA or dBSA films, were capped with Ni or Au electrodes with a thin Al_2O_3 tunneling barrier (Figure 6a). Due to preferential spin-polarized electron injection into the minority spin subbands and out of the majority spin subbands within ferromagnetic materials, dependence of the current on the magnetization orientation of the Ni electrode would indicate that the protein layers could polarize electron transport through the films. If Au rather than Ni capping electrodes are used, no significant difference of the current on an external magnetic field is expected.

The current between the top and bottom electrodes was measured while sweeping the voltage when an external magnetic field was applied underneath the devices to magnetize the top Ni electrodes up or down as shown in Figure 6a at room temperature. For each magnetic field orientation, 60 devices were tested on each of three independently prepared substrates (inset, Figure 6b), and the average current values for the three substrates are shown in Figure 6b. In each case, no significant differences in current were determined between field up *vs* field down conditions within the error of our measurements.

The characterization of similar device architectures was recently reported by Varade *et al.* in which the magnetoresistance of solid-state bacteriorhodopsin spin valves was measured.[59] While the native secondary structure of both bacteriorhodopsin and BSA contains multiple

α-helical subunits, unlike in BSA, the helices are well-aligned in bacteriorhodopsin, which likely enhances its ability to polarize transmitted electrons. Furthermore, the performance of the devices was enhanced when bacteriorhodopsin was treated with the use of detergents to stabilize protein secondary structure. Optimization of film deposition and device fabrication may enable the use of proteins within next-generation solid-state electrical components or spin valves.[2,60,61] However, our results suggest that neither BSA nor dBSA films can efficiently filter electrons within the conduction regime under the film preparation conditions used for these UPS measurements.

DISCUSSION

Mechanisms for Magnetization-Dependent Photoionization Energies.

We investigated substrate magnetization-dependent photoemission from FM substrates functionalized with chiral molecular assemblies. Others have reported experimental and theoretical investigations of the CISS effect, demonstrating electron helicity-dependent electron transmission in the low kinetic energy range of 0–2 eV.[18–21,24] Alternatively, no evidence of longitudinal spin polarization was found for photoelectrons with kinetic energies in the range of 30–760 eV transmitted through chiral DNA SAMs that were assembled on Au surfaces.[62] By UPS, we probe a previously untested photoelectron kinetic energy regime, and detect indirectly spin-dependent electron–chiral molecule interactions that may not necessarily lead to longitudinal spin filtering in transmission at all photoelectron energies.

We found that I for chiral molecular films depended on the magnetization orientation and polarization of the underlying FM metal. While photoionization of chiral molecules with unpolarized light is not a spin-selective process, we hypothesize that differences in I are related to the buildup of positive charges due to ionization by photoelectron impact. This hypothesis is consistent with the lack of significant interaction between magnetization orientation and photoemission angle for *L*-peptide films when measuring I (Figure 3f). Upon tilting the samples, the relative orientation between average electron spin in the FM metal and molecules remains unchanged, and while the degree of spin selectivity in photoemission may depend on the electron direction, the indirect effect of global changes in I would not be strongly influenced. Two potential explanations are enantioselective and electron helicity-dependent ionization cross sections in the films, and/or spin-dependent hole formation (Figure 7). Both mechanisms are rationalized by the emission of electrons with polarizations reflecting the average valence band polarization from the FM substrates, with kinetic energies above the ionization energies of the chiral molecules (7.2–7.3 eV). The inelastic mean free path of photoelectrons with kinetic energies between this threshold and the maximum kinetic energies probed in these experiments (16–18 eV) is expected to be <10 nm — short enough to permit scattering interactions with the adsorbed molecules (Table S3). However, spin-polarized photoelectrons capable of ionizing the molecules represent only a small fraction of the total photoelectron yield, which may account for the small measured differences in I.

Alternative explanations not involving photoelectron-induced ionization may influence *I* and could also be consistent with our results. Below, we consider and discuss these possibilities, the related data, and the consequences of each.

First, asymmetric scattering angles of photoelectrons depending on the handedness of the adsorbed chiral molecules may be manifested in ultraviolet photoelectron spectra. Asymmetric forward and backward scattering of photoelectrons emitted from gas-phase chiral molecules using circularly polarized ionizing radiation has been observed by circular dichroism in the angular distribution of photoelectrons.[63,64] This process is a result of pure electronic dipole transitions, and does not depend on spin-orbit coupling interactions. This phenomenon can be observed with achiral molecules as well, provided that they are oriented, [65] and the combined interactions between incident photons and molecular targets exhibit a defined handedness, which can be induced by precise experimental geometries.[25] However, because unpolarized radiation was used as an excitation source in our experiments, photoelectron circular dichroism is likely not responsible for the substrate magnetization-dependent effects described herein. Furthermore, the lack of dependence of *I* on substrate magnetization conditions for achiral, yet aligned, AUT SAMs on FM substrates also rules out this explanation.

Second, if the different surface charging, and thus *I*, that we measured between substrate magnetization orientations without charge neutralization were attributed to the capture of photoelectrons originating from the FM substrate with unfavorable helicity, then *I* and ϕ would be inversely related. Right-handed *L*-peptides assembled on Au have been shown to polarize transmitted photoelectrons with their spin oriented antiparallel to the surface normal.[20] Our UPS results with charge neutralization are consistent with these observations; lower ϕ when the substrates were magnetized up corresponds to a lower energy barrier to remove electrons from the surface when the spins of electrons within the majority spin subband are oriented antiparallel to the surface. When the substrates are magnetized down, a higher percentage of photoelectrons with their spins oriented parallel to the surface normal are emitted upon irradiation. Under these conditions, if more electrons do not escape the surface organic layer due to spin filtering than from surfaces magnetized in the opposite direction, then less charging, and lower *I*, would be expected when substrates were magnetized down. However, this prediction is not in agreement with our results, where lower *I* and ϕ values were measured when substrates were magnetized up.

Third, spin polarization of electrons transferred from the metal surface to neutralize holes within the organic layers may cause a buildup of positive charge in the film when the substrates are magnetized in the unfavorable orientation. When the majority electrons of the FM substrate do not match the preferred helicity in charge transfer, a higher resistance state results.[66] For *L*-peptide SAMs, right-handed electron helicity is preferred in the tunneling regime, that is, with spin aligned parallel to its linear momentum direction.[57] In our experimental setup, substrates magnetized down would provide favorable spin alignment for electrons transferred from the FM substrates to the organic films based only on the chirality of the peptides. This orientation would prevent the buildup of positive charge, resulting in lower *I* when substrates are magnetized down. However, this prediction does not match our

experimental results. Further, we found that dBSA films are not capable of filtering transferred electrons *via* conduction under the film conditions prepared for UPS measurements, eliminating this possible contribution to substrate magnetization-dependent surface charging in dBSA films.

Relating I and ϕ to Chiral-Induced Spin Selectivity in Photoelectron Transmission.

Interestingly, the trend in substrate magnetization orientation-dependence of I was reversed between α-helical *L*-peptide SAMs and dBSA films with high β-sheet content. If a higher I reflects a condition for larger scattering or ionization cross sections, our results suggest that photoelectrons transmitted through *L*-peptide SAMs and dBSA films are preferentially polarized with left- and right-handed helicity, respectively. The structure of surface-adsorbed BSA molecules represents a disorganized intermediate between these two systems, which may also explain the absence of the dependence of I on substrate magnetization conditions for BSA films on AUT SAMs. While both the peptides and proteins are composed of left-handed *L*-amino acid monomer subunits, we find that the secondary structure of the molecules dictate spin-selective interactions with transmitted electrons. These results corroborate studies on double-stranded *vs* single-stranded DNA.[8,18] While oligonucleotide strands of DNA contain *D*-deoxyribose sugars within the phosphodiester backbone, the handedness of the tertiary double-helix structure that results upon hybridization of complementary strands dictates the helicity preference in spin-selective interactions with electrons.

Further, at full saturation, the magnetization of the perpendicularly-magnetized FM substrates is still <100%. Therefore, the difference in ϕ of *ca.* 80 meV measured between opposite magnetization orientations with surface charge neutralization represents a *lower limit* of order-of-magnitude for the relative energy barrier to transmission of left- *vs* right-handed helicity electrons with energies above the vacuum level through α-helical peptide SAMs.

By comparison, spin-dependent energy barriers to transport through α-helical peptides in the conduction regime for electrons with energies below the vacuum level have been reported to be *ca.* 500 meV for peptides of approximately half the length of those used herein.[20] This value was determined by comparing the differences in the band gaps for the spin-density of states from dI/dV plots from conductive atomic force microscopy measurements of peptides assembled on Ni surfaces magnetized up *vs* down. The lower, relative energy barrier that we obtain in over-the-barrier transmission of photoelectrons through α-helical peptides may be attributed to the escape of electrons from regions devoid of SAM molecules due to inhomogeneous surface coverage, which would not depend on substrate magnetization condition.

Notably, under every measurement condition, no significant differences in the intensity, or counts, of photoelectrons collected, nor in the total integrated area considering photoelectrons of all kinetic energies (between 0 eV and *ca.* 18 eV, depending on the width of the spectra) were determined between substrates magnetized up *vs* down. In contrast, higher or lower intensities in electron energy distributions within the kinetic energy range of

~0–2 eV have been reported when Au substrates functionalized chiral films are irradiated with left- *vs* right-handed circularly polarized light to emit spin polarized electrons of opposite helicity from the Au surface.[18,24] In our measurements, photon energies are substantially larger than the ionization potential of the organic films ($h\nu \gg I$) and are likely insensitive to small (<1%) differences in I. Though, with surface charge neutralization, shifts in E_B^{max} are likely indicative of filtering of photoelectrons with low (< 0.5 eV) kinetic energies. While UPS enables the determination of relative energy barriers for photoemission of electrons with opposite helicity from chiral organic films, we could not conclusively identify differences in photoelectron yield using this technique.

Lastly, while we attribute the disappearance of magnetization-dependent effects when substrates were magnetized to sub-saturation conditions to the lower average polarization of electrons within the ferromagnetic material, we cannot rule out the possible effects of larger and more inhomogeneous stray magnetic fields at the surface compared to full saturation conditions due to the presence of domains.[67,68] Correlating experimental measurements of energy barriers to photoemission with new and evolving theoretical models that account for these variables will be critical to develop a foundational understanding of phenomena responsible for spin-selective transmission, ionization, and chiral-selective chemistries.[69,70]

CONCLUSIONS AND PROSPECTS

We investigated spin selectivity in photoemission from chiral molecular films assembled on ferromagnetic substrates using unpolarized ionizing radiation. Photoionization energies of α-helical peptides and films of thermally denatured proteins composed of *L*-amino acid monomers depended on underlying ferromagnetic substrate magnetization orientation and average polarization magnitude. While photoionization of chiral molecules with unpolarized light is not a spin-selective process, we attribute the observations to ionizing collisions from spin-polarized photoelectrons emitted from the underlying polarized surfaces. Furthermore, with surface charge neutralization, employed to deconvolute differential charging effects, we measured differences in work function between substrate magnetization conditions for α-helical *L*-peptide self-assembled monolayers. These differences are indicative of the relative electron helicity-dependent energy barriers to spin up *vs* spin down electron transmission through chiral films.

While the spin polarization of photoelectrons transmitted through chiral molecular assemblies may be measured using specialized experimental methods (*i.e.*, the use of a Mott polarimeter), this work establishes figures of merit to measure spin selectivity that can be assessed more readily and compared with varying molecular systems. Our experimental protocol to measure the magnetization-dependent photoionization energies and work functions of chiral molecular assemblies on ferromagnetic substrates is highly generalizable and will provide new mechanistic insight into spin-dependent interactions of electrons with chiral molecules.

Supplementary Material

Refer to Web version on PubMed Central for supplementary material.

ACKNOWLEDGMENTS

We gratefully acknowledge National Science Foundation ECCS Grant #1509794 for support of this work. KMC, CZ, and PSW also thank the National Institute on Drug Abuse (DA045550) for support. Work at UCSD was supported by National Science Foundation DMR Grant #1610538. JMA thanks UCLA for a Dissertation Year Fellowship. The authors acknowledge the use of instruments at the Nano and Pico Characterization Lab and the Integrated Systems Nanofabrication Cleanroom at the California NanoSystems Institute, and the UCLA Molecular Instrumentation Center. The authors thank Prof. Anne M. Andrews, Kristopher K. Barr, Dr. Ignacio Martini, Dr. Chris Moffitt, Prof. Ron Naaman, Dr. Nako Nakatsuka, Dr. Andrew C. Serino, and Matthew Ye for insightful discussions and their help.

REFERENCES

1. Michaeli K; Kantor-Uriel N; Naaman R; Waldeck DH The Electron's Spin and Molecular Chirality – How Are They Related and How Do They Affect Life Processes? Chem. Soc. Rev. 2016, 45, 6478–6487. [PubMed: 27734046]
2. Michaeli K; Varade V; Naaman R; Waldeck DH A New Approach towards Spintronics: Spintronics with No Magnets. J. Phys.: Condens. Matter 2017, 29, 103002.
3. Naaman R; Waldeck DH Chiral-Induced Spin Selectivity Effect. J. Phys. Chem. Lett. 2012, 3, 2178–2187. [PubMed: 26295768]
4. Mondal PC; Fontanesi C; Waldeck DH; Naaman R Spin-Dependent Transport through Chiral Molecules Studied by Spin-Dependent Electrochemistry. Acc. Chem. Res. 2016, 49, 2560–2568. [PubMed: 27797176]
5. Fontanesi C; Capua E; Paltiel Y; Waldeck DH; Naaman R Spin-Dependent Processes Measured without a Permanent Magnet. Adv. Mater. 2018, 99, 1707390.
6. Mayer S; Kessler J Experimental Verification of Electron Optic Dichroism. Phys. Rev. Lett. 1995, 74, 4803–4806. [PubMed: 10058603]
7. Nolting C; Mayer S; Kessler J Electron Dichroism – New Data and an Experimental Cross-Check. J. Phys. B: At. Mol. Opt. Phys. 1997, 30, 5491–5499.
8. Zwang TJ; Hürlimann S; Hill MG; Barton JK Helix-Dependent Spin Filtering through the DNA Duplex. J. Am. Chem. Soc. 2016, 138, 15551–15554. [PubMed: 27934017]
9. Mondal PC; Roy P; Kim D; Fullerton EE; Cohen H; Naaman R Photospintronics: Magnetic Field-Controlled Photoemission and Light-Controlled Spin Transport in Hybrid Chiral Oligopeptide-Nanoparticle Structures. Nano Lett. 2016, 16, 2806–2811. [PubMed: 27027885]
10. Eckshtain-Levi M; Capua E; Refaely-Abramson S; Sarkar S; Gavrilov Y; Mathew SP; Paltiel Y; Levy Y; Kronik L; Naaman R Cold Denaturation Induces Inversion of Dipole and Spin Transfer in Chiral Peptide Monolayers. Nat. Commun. 2016, 7, 10744. [PubMed: 26916536]
11. Bloom BP; Graff BM; Ghosh S; Beratan DN; Waldeck DH Chirality Control of Electron Transfer in Quantum Dot Assemblies. J. Am. Chem. Soc. 2017, 139, 9038–9043. [PubMed: 28609095]
12. Mtangi W; Tassinari F; Vankayala K; Jentzsch AV; Adelizzi B; Palmans ARA; Fontanesi C; Meijer EW; Naaman R Control of Electrons' Spin Eliminates Hydrogen Peroxide Formation during Water Splitting. J. Am. Chem. Soc. 2017, 139, 2794–2798. [PubMed: 28132505]
13. Abendroth JM; Nakatsuka N; Ye M; Kim D; Fullerton EE; Andrews AM; Weiss PS Analyzing Spin Selectivity in DNA-Mediated Charge Transfer via Fluorescence Microscopy. ACS Nano 2017, 11, 7516–7526. [PubMed: 28672111]
14. Kumar A; Capua E; Kesharwani K; Martin JML; Sitbon E; Waldeck DH; Naaman R. Chirality-Induced Spin Polarization Places Symmetry Constraints on Biomolecular Interactions. Proc. Natl. Acad. Sci. U. S. A. 2017, 114, 2474–2478. [PubMed: 28228525]
15. Dor OB; Yochelis S; Radko A; Vankayala K; Capua E; Capua A; Yang S-H; Baczewski LT; Parkin SSP; Naaman R; Paltiel Y Magnetization Switching in Ferromagnets by Adsorbed Chiral Molecules without Current or External Magnetic Field. Nat. Commun. 2017, 8, 14567. [PubMed: 28230054]
16. Banerjee-Ghosh K; Dor OB; Tassinari F; Capua E; Yochelis S; Capua A; Yang S-H; Parkin SSP; Sarkar S; Kronik L; Baczewski LT; Naaman R; Paltiel Y Separation of Enantiomers by their

Enantiospecific Interactions with Achiral Magnetic Substrates. Science 2018, 360, 1331–1334. [PubMed: 29748324]

17. Santos JI; Rivilla I; Cossio FP; Matxain JM; Grzelczak M; Mazinani SKS; Ugalde JM; Mujica V Chirality-Induced Electron Spin Polarization and Enantiospecific Response in Solid State Cross-Polarization Nuclear Magnetic Resonance. ACS Nano 2018 DOI: 10.1021/acsnano.8b06467.
18. Göhler B; Hamelbeck V; Markus TZ; Kettner M; Hanne GF; Vager Z; Naaman R; Zacharias H Spin Selectivity in Electron Transmission through Self-Assembled Monolayers of Double-Stranded DNA. Science 2011, 331, 894–897. [PubMed: 21330541]
19. Mishra D; Markus TZ; Naaman R; Kettner M; Göhler B; Zacharias H; Friedman N; Sheves M; Fontanesi C Spin-Dependent Electron Transmission through Bacteriorhodopsin Embedded in Purple Membrane. Proc. Natl. Acad. Sci. U. S. A. 2013, 110, 14872–14876. [PubMed: 23980184]
20. Kettner M; Göhler B; Zacharias H; Mishra D; Kiran V; Naaman R; Fontanesi C; Waldeck DH; Sęk S; Pawłowski J; Juhaniewicz J Spin Filtering in Electron Transport through Chiral Oligopeptides. J. Phys. Chem. C 2015, 119, 14542–14547.
21. Kettner M; Maslyuk VV; Nürenberg D; Seibel J; Gutierrez R; Cuniberti G; Ernst K–H; Zacharias H Chirality-Dependent Electron Spin Filtering by Molecular Monolayers of Helicenes. J. Phys. Chem. Lett. 2018, 9, 2025–2030. [PubMed: 29618210]
22. Polarized Electrons in Surface Physics, Vol. 1; Feder R, Ed.; World Scientific: Singapore, 1985.
23. Kisker E; Gudat W; Schröder K Observation of a High Spin Polarization of Secondary Electrons from Single Crystal Fe and Co. Solid State Commun. 1982, 44, 591–595.
24. Ray K; Ananthavel SP; Waldeck DH; Naaman R Asymmetric Scattering of Polarized Electrons by Organized Organic Films of Chiral Molecules. Science 1999, 283, 814–816. [PubMed: 9933157]
25. Schönhense G Circular Dichroism and Spin Polarization in Photoemission from Adsorbates and Non-Magnetic Solids. Physica Scripta 1990, T31, 255–275.
26. Heizmann U; Schönhense G; Kessler J Polarization of Photoelectrons Ejected by Unpolarized Light from Xenon Atoms. Phys. Rev. Lett. 1979, 42, 1603–1605.
27. Jones S; Madison DH; Hanne GF Spin-Resolved (e, 2e) Coincidences for Heavy Rare-Gas Targets. Phys. Rev. Lett. 1994, 72, 2554–2556. [PubMed: 10055913]
28. Guo X; Hurn JM; Lower J; Mazevet S; Shen Y; Weigold E; Granitza B; McCarthy IE Fine Structure Effect in Electron Impact Ionization. Phys. Rev. Lett. 1996, 76, 1228–1231. [PubMed: 10061668]
29. Kumar KS; Kantor-Uriel N; Mathew SP; Guliamov R; Naaman R A Device for Measuring Spin Selectivity in Electron Transfer. Phys. Chem. Chem. Phys. 2013, 15, 18357–18362. [PubMed: 24077104]
30. Kim J; Rim YS; Liu Y; Serino AC; Thomas JC; Chen H; Yang Y; Weiss PS Interface Control in Organic Electronics using Mixed Monolayers of Carboranethiol Isomers. Nano Lett. 2014, 14, 2946–2951. [PubMed: 24773449]
31. Cabarcos OM; Schuster S; Hehn I; Zhang PP; Maitani MM; Sullivan N; Giguère J-B; Morin J-F; Weiss PS; Zojer E; Zharnikov M; Allara DL. Effects of Embedded Dipole Layers on Electrostatic Properties of Alkanethiolate Self-Assembled Monolayers. J. Phys. Chem. C 2017, 121, 15815–15830.
32. Serino AC; Anderson ME; Saleh LMA; Dziedzic RM; Mills H; Heidenreich LK; Spokoyny AM; Weiss PS Work Function Control of Germanium through Carborane-Carboxylic Acid Surface Passivation. ACS Appl. Mater. Interfaces 2017, 9, 34592–34596. [PubMed: 28920673]
33. Yeganah S; Ratner MA; Medina E; Mujica V Chiral Electron Transport: Scattering through Helical Potentials. J. Chem. Phys. 2009, 131, 014707.
34. Gutierrez R; Díaz E; Naaman R; Cuniberti G Spin Selective Transport through Helical Molecular Systems. Phys. Rev. B 2012, 85, 081404.
35. Vager D; Vager Z Spin Order without Magnetism: A New Phase of Spontaneously Broken Symmetry in Condensed Matter. Phys. Lett. A 2012, 376, 1895–1897.
36. Gutierrez R; Díaz E; Gaul C; Brumme T; Domínguez-Adame F; Cuniberti G Modeling Spin Transport in Helical Fields: Derivation of an Effective Low-Dimensional Hamiltonian. J. Phys. Chem. C 2013, 117, 22276–22284.

37. Gersten J; Kaasbjerg K; Nitzan A Induced Spin Filtering in Electron Transmission through Chiral Molecule Layers Adsorbed on Metals with Strong Spin-Orbit Coupling. J. Chem. Phys. 2013, 139, 114111.
38. Eremko AA; Loktev VM Spin Sensitive Electron Transmission through Helical Potentials. Phys. Rev. B 2013, 88, 165409.
39. Guo AM; Sun QF Spin-Dependent Electron Transport in Protein-Like Single-Helical Molecules. Proc. Natl. Acad. Sci. USA 2014, 111, 11658–11662. [PubMed: 25071198]
40. Medina E; González-Arraga LA; Finkelstein-Shapiro D; Berche B; Mujica V Continuum Model for Chiral Induced Spin Selectivity in Helical Molecules. J. Chem. Phys. 2015, 142, 194308–194313. [PubMed: 26001462]
41. Sykes ECH; Mantooth BA; Han P; Donhauser ZJ; Weiss PS Substrate-Mediated Intermolecular Interactions: A Quantitative Single Molecule Analysis. J. Am. Chem. Soc. 2005, 127, 7255–7260. [PubMed: 15884967]
42. Zaera F Chirality in Adsorption on Solid Surfaces. Chem. Soc. Rev. 2017, 46, 7374–7398. [PubMed: 29043322]
43. Stranick SJ; Parikh AN; Allara DL; Weiss PS A New Mechanism for Surface Diffusion: Motion of a Substrate-Adsorbate Complex. J. Phys. Chem. 1994, 98, 11136–11142.
44. Stranick SJ; Parikh AH; Tao Y-T; Allara DL; Weiss PS Phase Separation of Mixed-Composition Self-Assembled Monolayers into Nanometer Scale Molecular Domains. J. Phys. Chem. 1994, 98, 7636–7646.
45. Bumm LA; Arnold JJ; Charles LF; Dunbar TD; Allara DL; Weiss PS Directed Self-Assembly to Create Molecular Terraces with Molecularly Sharp Boundaries in Organic Monolayers. J. Am. Chem. Soc. 1999, 121, 8017–8021.
46. Medina E; Lopez F; Ratner MA Mujica, V. Chiral Molecular Films as Electron Polarizers and Polarization Modulators. Europhys. Lett. 2012, 99, 17006.
47. Goronzy DP; Ebrahimi M; Rosei F; Arramel Fang, Y.; De Feyter S; Tait SL; Wang C; Beton PH; Wee ATS; Weiss PS; Perepichka DF Supramolecular Assemblies on Surfaces: Nanopatterning, Functionality, and Reactivity. ACS Nano 2018, 12, 7445–7481. [PubMed: 30010321]
48. Kim J; Somorjai GA Molecular Packing of Lysozyme, Fibrinogen, and Bovine Serum Albumin on Hydrophilic and Hydrophobic Surfaces Studied by Infrared-Visible Sum Frequency Generation and Fluorescence Microscopy. J. Am. Chem. Soc. 2003, 125, 3150–3158. [PubMed: 12617683]
49. Jeyachandran YL; Mielczarski E; Rai B; Mielczarski JA Quantitative and Qualitative Evaluation of Adsorption/Desorption of Bovine Serum Albumin on Hydrophilic and Hydrophobic Surfaces. Langmuir 2009, 25, 11614–11620. [PubMed: 19788219]
50. Phan HTM; Bartelt-Hunt S; Rodenhausen KB; Schubert M; Bartz JC Investigation of Bovine Serum Albumin (BSA) Attachment onto Self-Assembled Monolayers (SAMs) using Combinatorial Quartz Crystal Microbalance with Dissipation (QCM-D) and Spectroscopic Ellipsometry (SE). PLoS One 2015, 10, 0141282.
51. Norde W; Giacomelli CE BSA Structural Changes during Homomolecular Exchange between the Adsorbed and the Dissolved States. J. Biotechnol. 2000, 79, 259–268. [PubMed: 10867186]
52. Militello V; Casarino C; Emanuele A; Giostra A; Pullara F; Leone M Aggregation Kinetics of Bovine Serum Albumin Studied by FTIR Spectroscopy and Light Scattering. Biophys. Chem. 2004, 107, 175–187. [PubMed: 14962598]
53. Moriyama Y; Watanabe E; Kobayashi K; Harano H; Inui E; Takeda K Secondary Structural Change of Bovine Serum Albumin in Thermal Denaturation up to 130 ºC and Protective Effect of Sodium Dodecyl Sulfate on the Change. J. Phys. Chem. B 2008, 112, 16585–16589. [PubMed: 19367984]
54. Roach P; Farrar D; Perry CC Interpretation of Protein Adsorption: Surface-Induced Conformational Changes. J. Am. Chem. Soc. 2005, 127, 8168–8173. [PubMed: 15926845]
55. Larson PE; Kelly MA. Surface Charge Neutralization of Insulating Samples in X-Ray Photoemission Spectroscopy. J. Vac. Sci. Technol. A 1998, 16, 3483–3489.
56. McArthur SL; Mishra G; Easton CD Applications of XPS in Biology and Biointerface Analysis In Surface Analysis and Techniques in Biology; Smentkowski V. Ed.; Springer, Cham, 2014; pp 9–36.

57. Aragonès AC; Medina E; Ferrer-Huerta M; Gimeno N; Teixidó M; Palma JL; Tao N; Ugalde JM; Giralt E; Díez-Pérez I; Mujica V Measuring the Spin-Polarization Power of a Single Chiral Molecule. Small 2017, 13, 1602519.
58. Tassinari F; Jayarathna DR; Kantor-Uriel N; Davis KL; Varade V; Achim C; Naaman R Chirality Dependent Charge Transfer Rate in Oligopeptides. Adv. Mater. 2018, 30, 1706423.
59. Varade V; Markus T; Vankayala K; Friedman N; Sheves M; Waldeck DH; Naaman R Bacteriorhodopsin-Based Non-Magnetic Spin Filters for Biomolecular Spintronics. Phys. Chem. Chem. Phys. 2018, 20, 1091–1097. [PubMed: 29238765]
60. Amdursky N; Marchak D; Sepunaru L; Pecht I; Sheves M; Cahen D Electronic Transport via Proteins. Adv. Mater. 2014, 26, 7142–7161. [PubMed: 25256438]
61. Vilan A; Aswal D; Cahen D Large-Area, Ensemble Molecular Electronics: Motivation and Challenges. Chem. Rev. 2017, 117, 4248–4286. [PubMed: 28177226]
62. Rosenberg RA; Symonds JM; Kalyanaraman V; Markus T; Orlando TM; Naaman R; Medina EA; López FA; Mujica V Kinetic Energy Dependence of Spin Filtering of Electrons Transmitted through Organized Layers of DNA. J. Phys. Chem. C 2013, 117, 22307–22313.
63. Böwering N; Lischke T; Schmidtke B; Müller N; Khalil T; Heinzmann U Asymmetry in Photoelectron Emission from Chiral Molecules Induced by Circularly Polarized Light. Phys. Rev. Lett. 2001, 86, 1187–1190. [PubMed: 11178040]
64. Turchini S; Zema N; Contini G; Alberti G; Alagia M; Stranges S; Fronzoni G; Stener M; Decleva P; Prosperi T Circular Dichroism in Photoelectron Spectroscopy of Free Chiral Molecules: Experiment and Theory on Methyl-Oxirane. Phys. Rev. A 2004, 70, 014502.
65. Dubs RL; Dixit SN; McKoy V Circular Dichroism in Photoelectron Angular Distributions from Oriented Linear Molecules. Phys. Rev. Lett. 1985, 54, 1249–1251. [PubMed: 10030976]
66. Maslyuk VV; Gutierrez R; Dianat A; Mujica V; Cuniberti G Enhanced Magnetoresistance in Chiral Molecular Junctions. J. Phys. Chem. Lett. 2018, 9, 5453–5459. [PubMed: 30188726]
67. Kittel C Physical Theory of Ferromagnetic Domains. Rev. Mod. Phys. 1949, 21, 541–583.
68. Kooy C; Enz U Experimental and Theoretical Study of the Domain Configuration in Thin Layers of $BaFe_{12}O_{19}$. Philips Res. Repts. 1960, 15, 7–29.
69. Rosenberg RA; Haija MA; Ryan PJ Chiral-Selective Chemistry Induced by Spin-Polarized Secondary Electrons from a Magnetic Substrate. Phys. Rev. Lett. 2008, 101, 178301. [PubMed: 18999792]
70. Rosenberg RA; Mishra D; Naaman R Chiral Selective Chemistry Induced by Natural Selection of Spin-Polarized Electrons. Angew. Chem. Int. Ed. 2015, 54, 7295–7298.

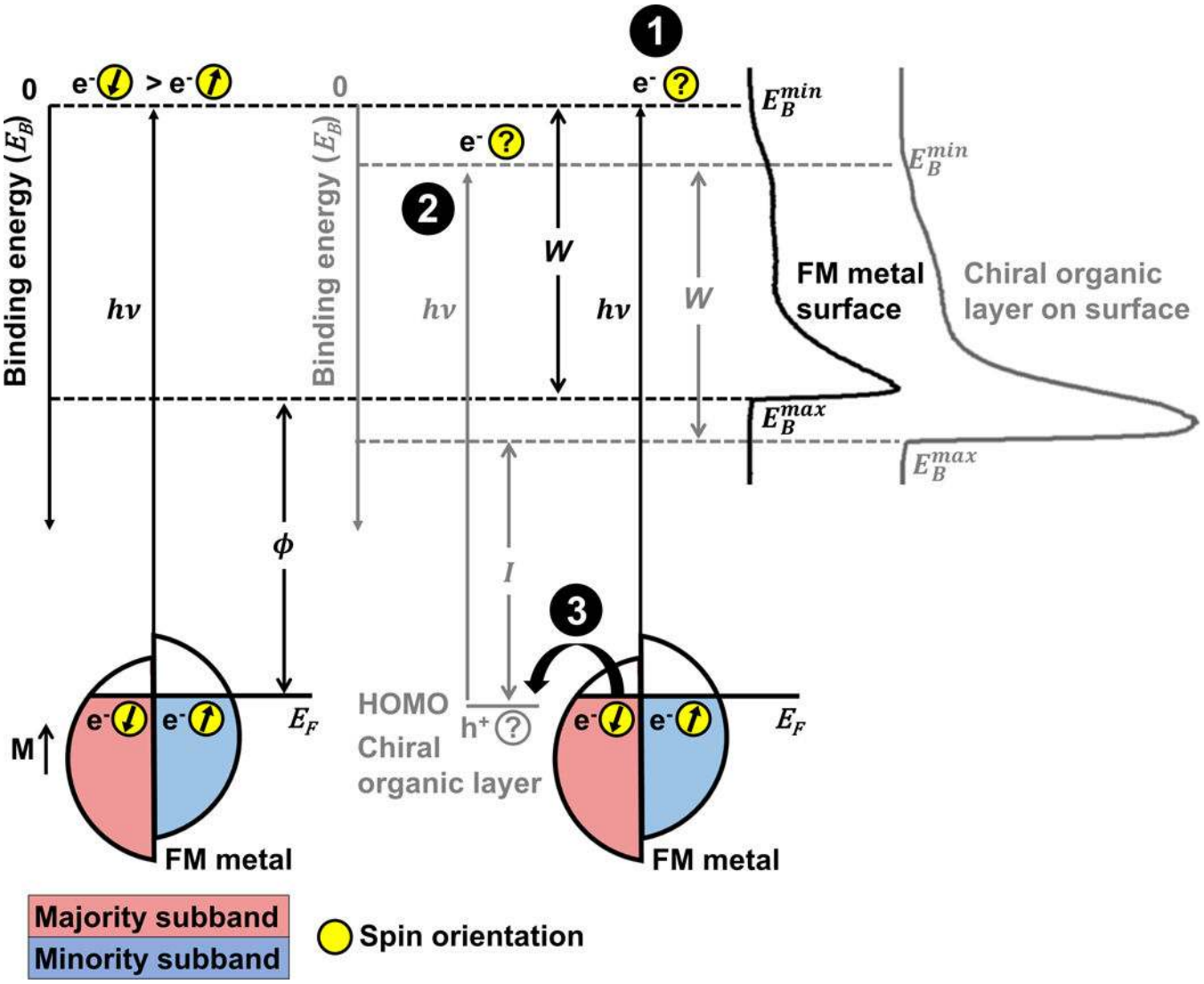

Figure 1:

Experimental schematic of ultraviolet photoelectron spectroscopy (UPS) of ferromagnetic multilayer (FM) metal surfaces. Spin-selective processes due to the chiral-induced spin selectivity effect may include filtering of photoelectrons originating from the metal by adsorbed chiral species (1), spin-polarized photoemission by ionization of chiral films (2), or filtering of conduction electrons supplied by the metal to fill holes left in the valence orbitals of the organic films, represented schematically as the highest occupied molecular orbitals (HOMO) (3). The right side of the image depicts representative ultraviolet photoelectron spectra from bare FM surfaces (black) and surfaces coated with chiral organic films (grey). The large peaks at high binding energies correspond to the collection of secondary electrons that scatter, losing energy. The spin polarization of photoelectrons emitted from bare FM surfaces by photons with energy $h\nu$ reflects the polarization within the metal dictated by the magnetization orientation, M. The Fermi edge and minimum binding energy, E_B^{min}, of the metal is at 0 eV, and the secondary electron cutoff of electrons with maximum binding

energy is E_B^{max}. When functionalized with organic chiral layers, photoelectrons are collected from both the metal surface as well as the organic material due to ionization. The valence band edge of the spectra, E_B^{min}, and the secondary electron cutoff, E_B^{max}, represent the highest and lowest kinetic energies of collected photoelectrons, respectively. The minimum energy required to remove an electron from the surface is the work function, ϕ. The spectral width, W, is used to calculate the photoionization energy, I, of the organic films.

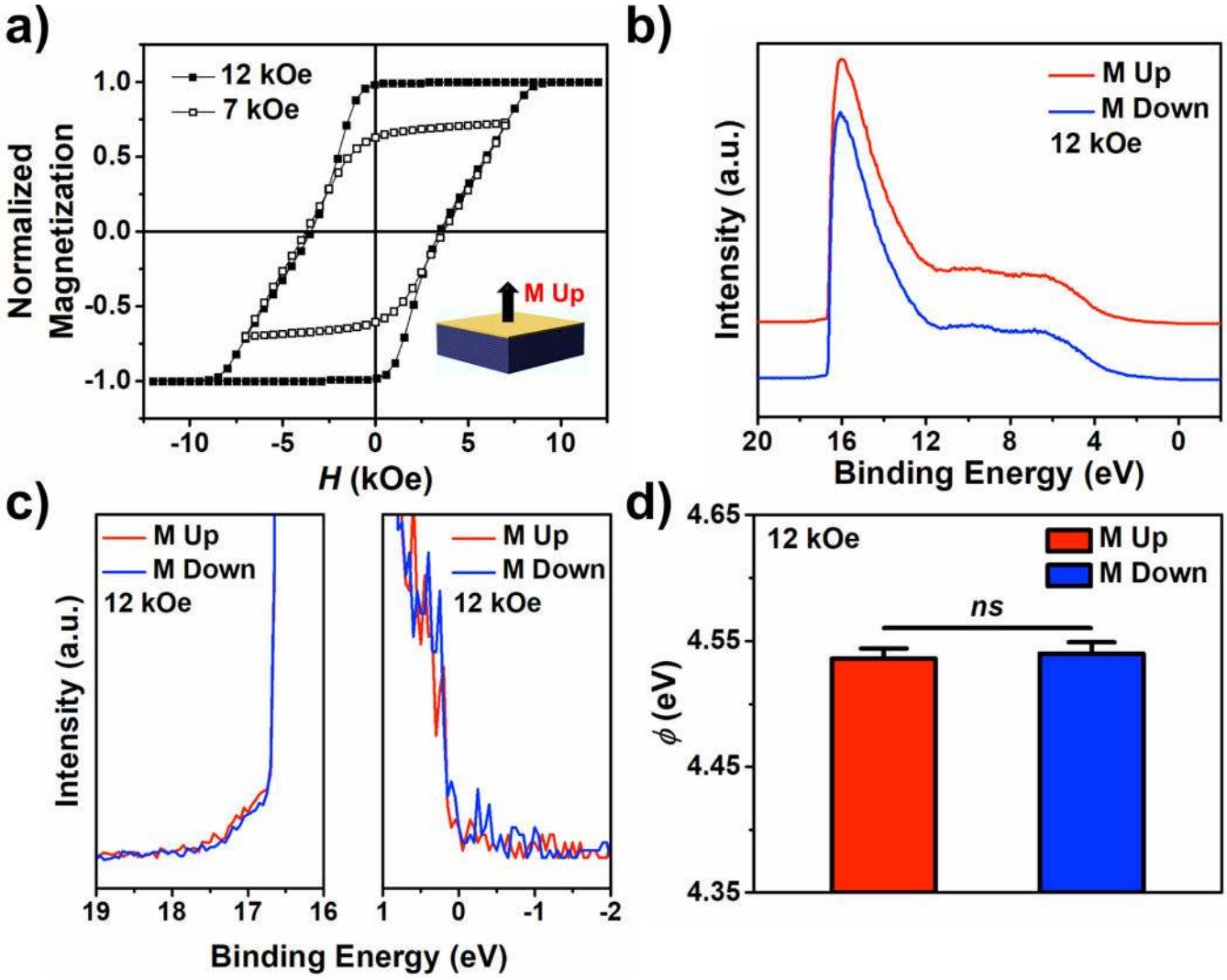

Figure 2:

Characterization of bare ferromagnetic multilayer (FM) films with composition: glass substrate/Ta 3/Pt 2/$[Co\ 0.6/Pt\ 0.3]_{69}$/Co 0.6/Au 1 (layers in nm). **a**) Hysteresis loops of FM substrates with ±12 kOe and ±7 kOe saturating magnetic fields (H). **b**) Representative full ultraviolet photoelectron spectra of bare substrates magnetized up (red) or down (blue) at full saturation using a helium-ion ultraviolet light source (He I). Spectra obtained from substrates magnetized up *vs* down are offset for clarity. **c**) Magnification of the secondary electron cutoff regions and Fermi edges of the spectra in **b**). **d**) Work function values of the surfaces magnetized up (red) or down (blue) at full saturation calculated from the ultraviolet photoelectron spectra. Error bars represent standard errors of the means; *ns* is not significant ($P > 0.05$).

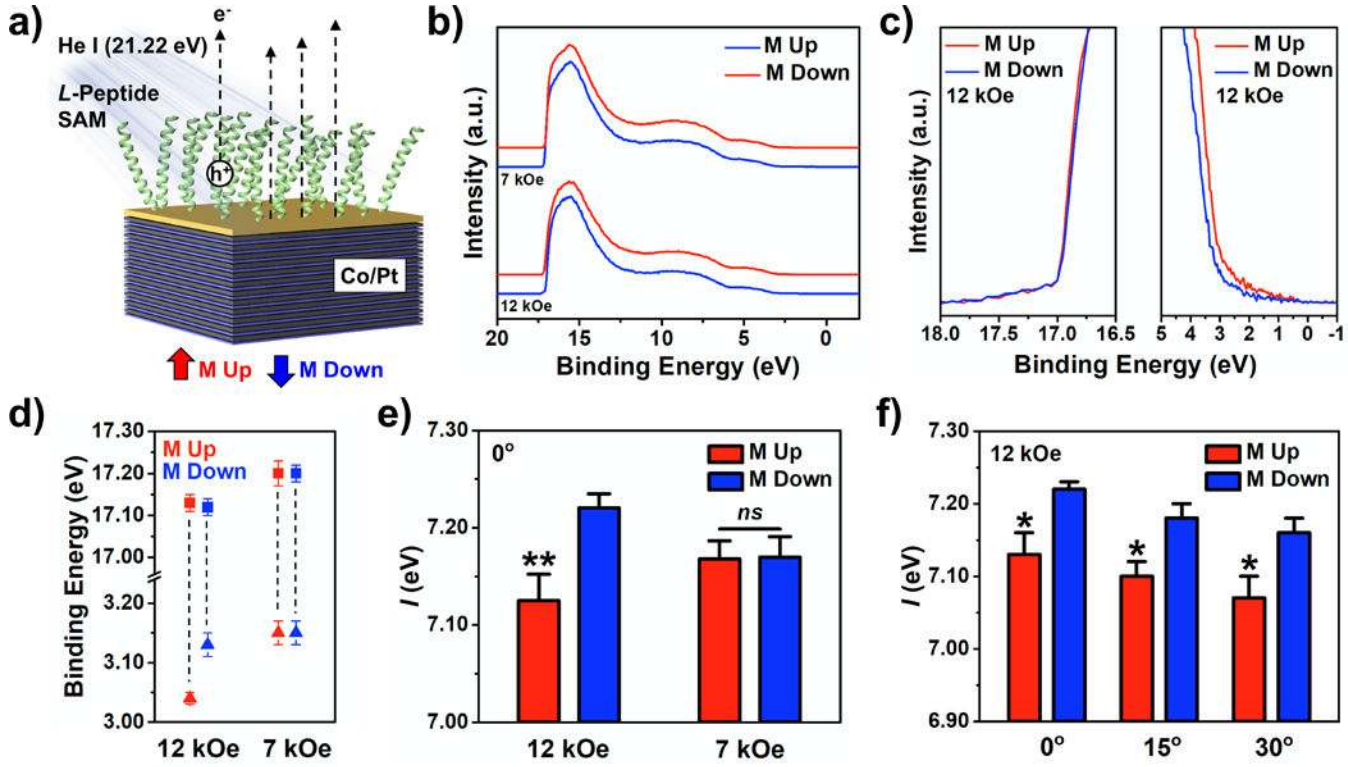

Figure 3:

Characterization of ferromagnetic multilayer (FM) substrates functionalized with self-assembled monolayers (SAMs) of *L*-peptides by ultraviolet photoelectron spectroscopy using a helium-ion ultraviolet light source (He I). **a**) Experimental schematic for two opposite (up *vs* down) magnetization orientations. **b**) Full, representative photoelectron spectra for *L*-peptide SAMs on FM substrates magnetized with ±12 or ±7 kOe. Spectra obtained from substrates magnetized up *vs* down are offset for clarity. **c**) Magnification of the secondary electron cutoff regions and valence band edges of representative spectra obtained for substrates magnetized to full saturation. **d**) Secondary electron cutoffs (squares) and valence band edges (triangles) for *L*-peptide SAMs on substrates magnetized to full- and sub-saturation. **e**) Photoionization energies of *L*-peptide SAMs on FM substrates magnetized up *vs* down at full- and sub-saturation magnetization. **f**) Photoionization energies measured for *L*-peptide SAMs on FM substrates magnetized up *vs* down at full magnetic saturation when photoelectrons were collected at angles of 0°, 15°, and 30° relative to the surface normal. Error bars represent standard errors of the means; $*P < 0.05$ *vs* M down; $**P < 0.01$ *vs* M down; *ns* is not significant ($P > 0.05$).

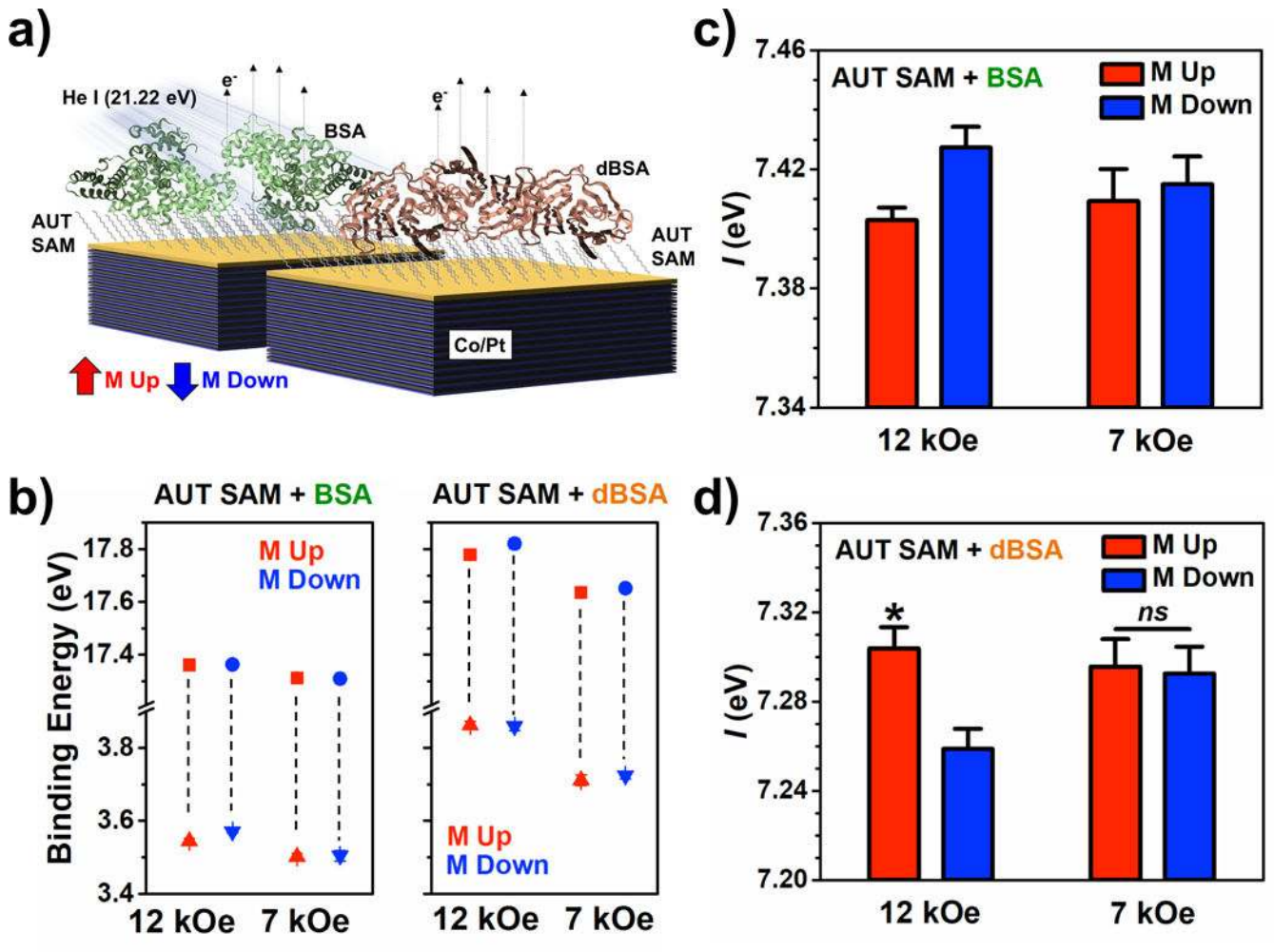

Figure 4:

Characterization of ferromagnetic multilayer (FM) substrates functionalized with self-assembled monolayers (SAMs) of 11-amino-1-undecanethiol (AUT) and films of bovine serum albumin (BSA) or thermally denatured bovine serum albumin (dBSA) by ultraviolet photoelectron spectroscopy using a helium-ion ultraviolet light source (He I). **a**) Experimental schematic. **b**) Secondary electron cutoffs (squares) and valence band edges (triangles) for AUT SAMs with BSA (left) or dBSA films (right) on substrates magnetized to full- *vs* sub-saturation magnetization. **c**) Photoionization energies of FM substrates magnetized up *vs* down at full- and sub-saturation magnetization for AUT SAMs with BSA and **d**) dBSA. For the AUT SAM + BSA condition, no significance was determined in the interaction term or main effects from two-way analysis of variance, so *post hoc* tests were not performed. Error bars represent standard error of the means; $*P < 0.05$ *vs* M down; *ns* is not significant ($P > 0.05$).

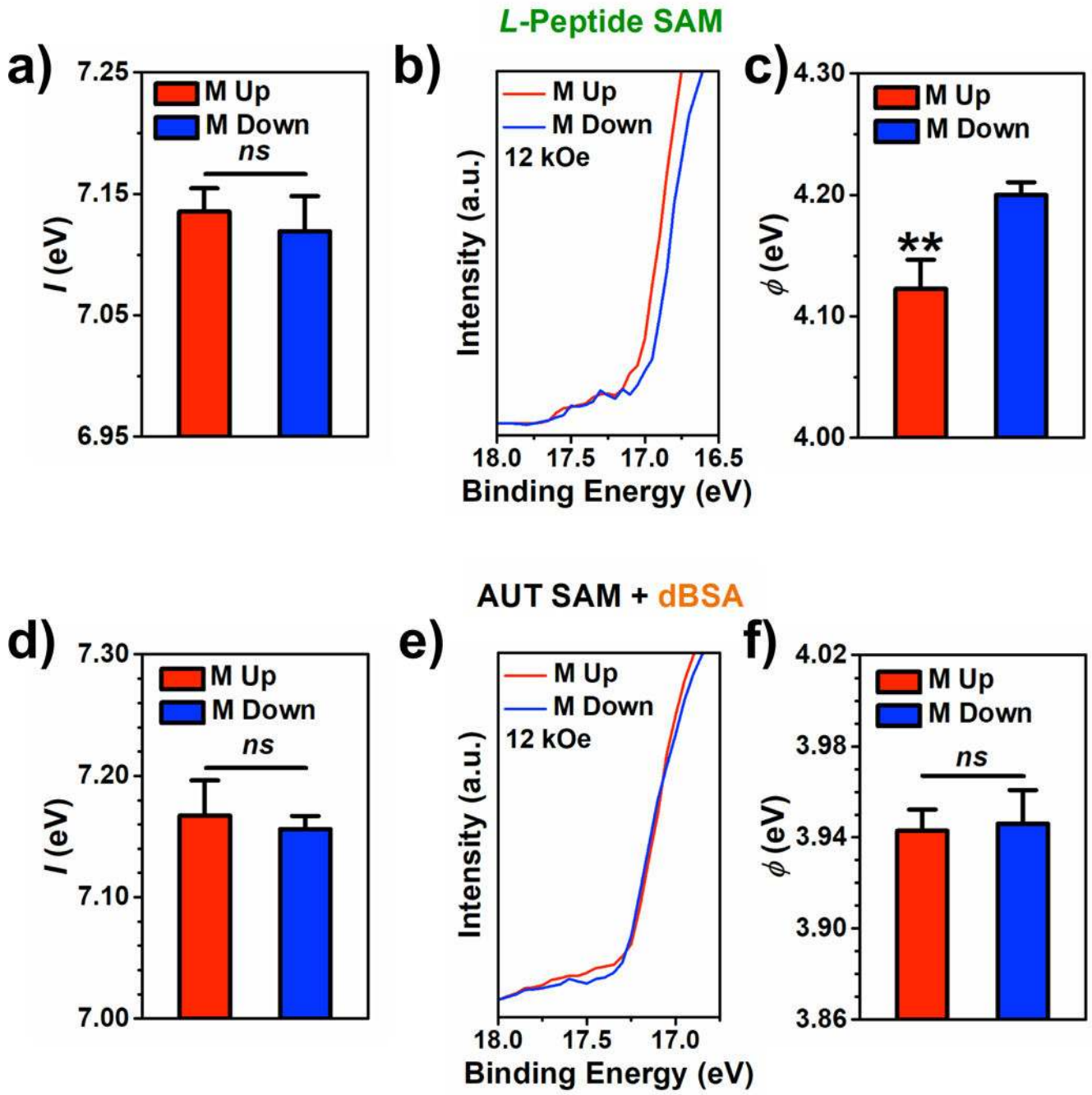

Figure 5:

Characterization of ferromagnetic multilayer (FM) substrates functionalized with *L*-peptide self-assembled monolayers (SAMs) and SAMs of 11-amino-1-undecanethiol (AUT) with films of thermally denatured bovine serum albumin (dBSA) by ultraviolet photoelectron spectroscopy using a helium-ion ultraviolet light source (He I) under charge neutralization conditions and full magnetization saturation. **a**) Photoionization energy of *L*-peptide SAMs on FM substrates magnetized up *vs* down. **b**) Magnified region of the secondary electron cutoff of representative photoelectron spectra from FM substrates functionalized with *L*-

peptide SAMs magnetized up *vs* down. **c**) Work function values of FM substrates magnetized up *vs* down for *L*-peptide SAMs. **d-f**) Analogous results for FM substrates functionalized with AUT SAMs + dBSA. Error bars represent standard error of the means; $^{**}P < 0.01$ *vs* M down; *ns* is not significant ($P > 0.05$).

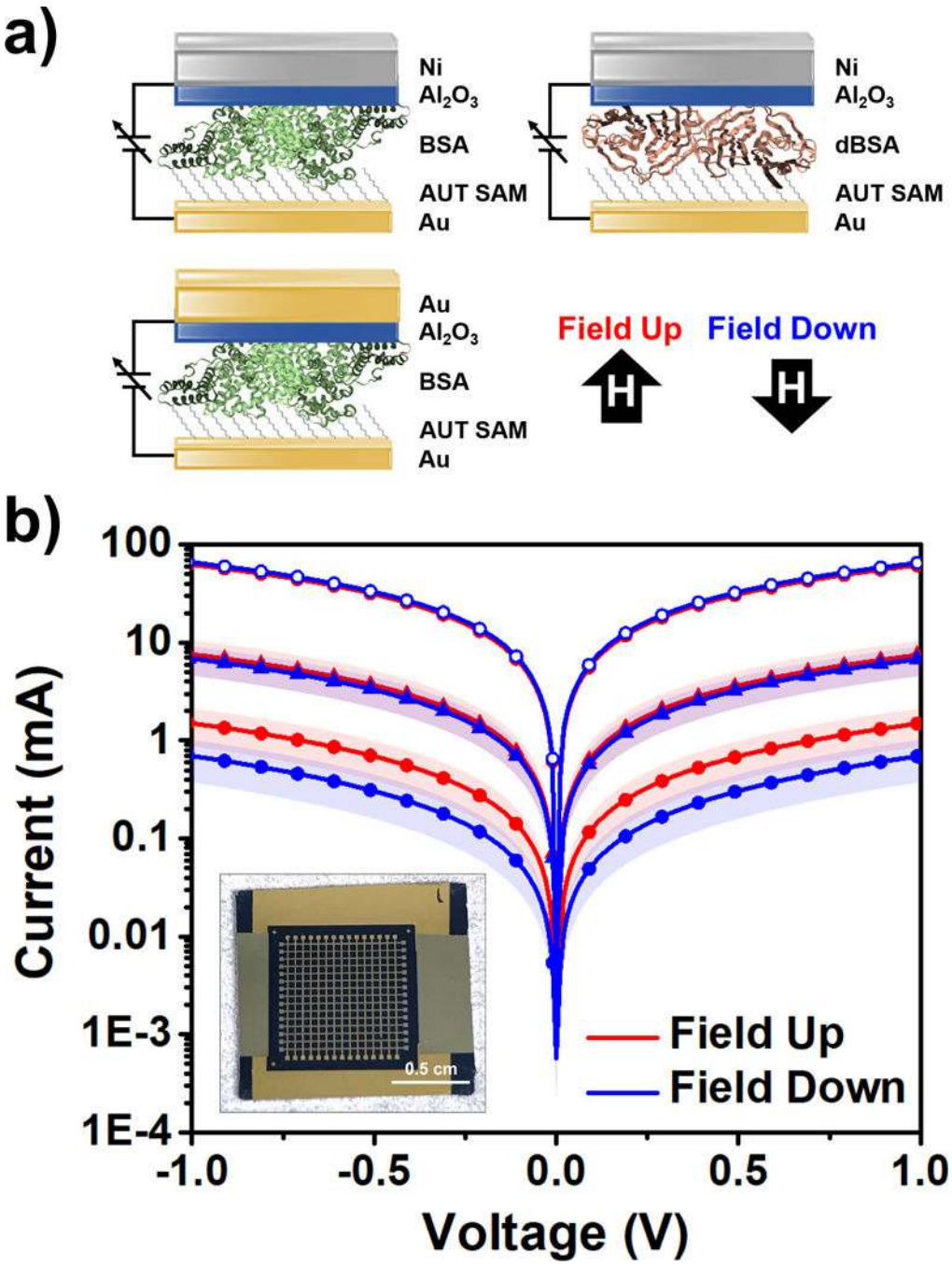

Figure 6:

a) Schematic of spin-valve device architectures composed of self-assembled monolayers (SAMs) of 11-amino-1-undecanethiol (AUT) and electrostatically adsorbed films of bovine serum albumin (BSA) or thermally denatured bovine serum albumin (dBSA) sandwiched between non-ferromagnetic Au and ferromagnetic Ni electrodes. An external magnetic field is used to magnetize the Ni electrodes parallel or antiparallel to the normal axis of the devices. **b**) Average current-voltage measurements for Au/BSA/Ni (solid circles), Au/dBSA/Ni (solid triangles), and Au/BSA/Au (open circles) junctions from three substrates

(photograph in inset). Shaded areas represent standard error of the mean from N=3 substrates for each condition (n=60 panels tested per magnetic field orientation per substrate).

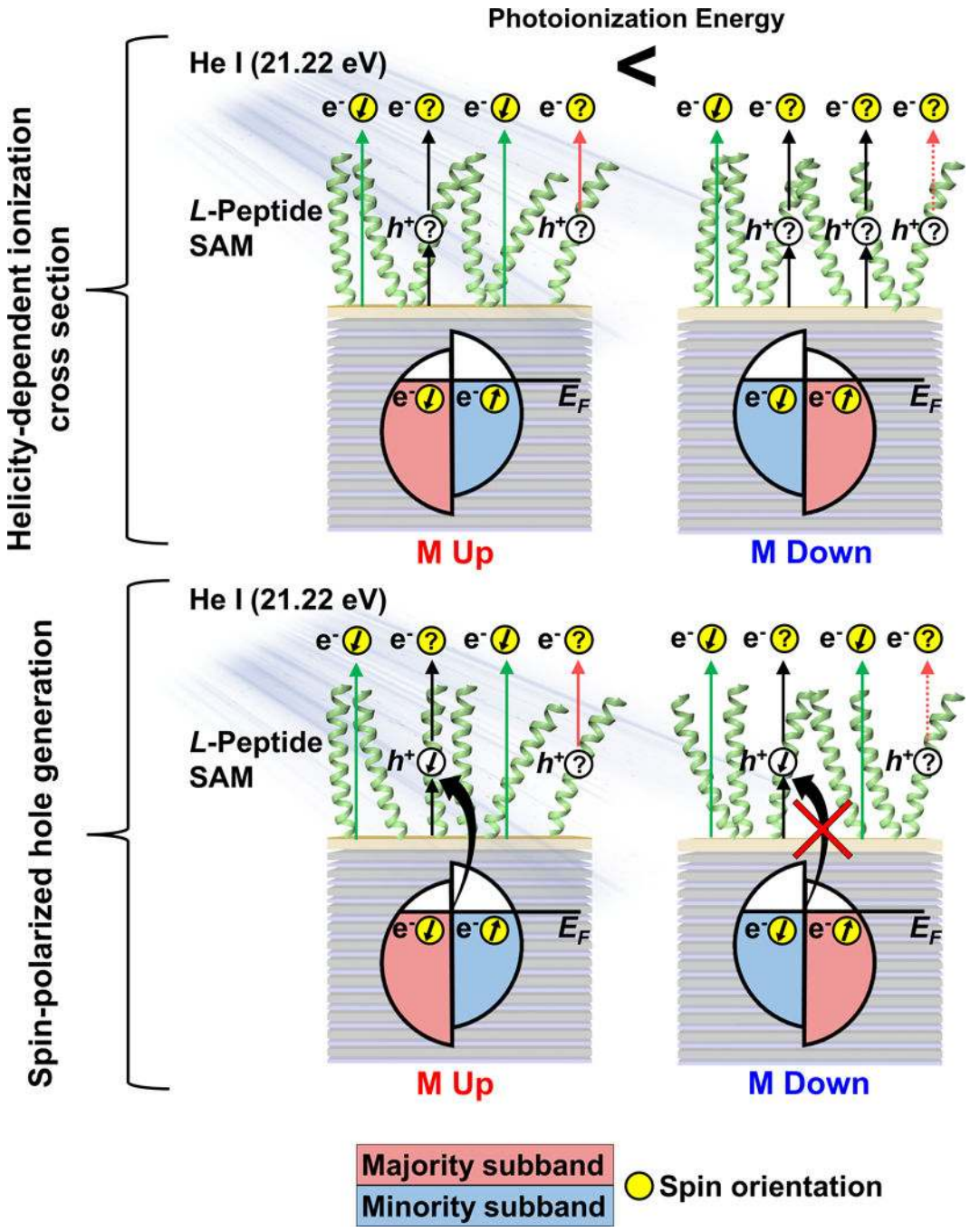

Figure 7:

Schematic representing possible mechanisms to describe substrate magnetization-dependent photoionization energies of chiral self-assembled monolayers (SAMs) on ferromagnetic multilayer (FM) substrates. Greater buildup of positive charge in the organic layers when substrates are magnetized down *vs* up effectively increases the photoionization energy. Green arrows represent photoemission originating from the FM substrates. For *L*-peptide SAMs, transmitted photoelectrons are expected to be polarized with left-handed helicity, regardless of initial polarization. Black double arrows represent molecular ionization by

impact of photoelectrons with sufficient energy from the FM substrates, a spin-selective process. Pink arrows represent photoemission by direct photoionization of molecules, the efficiency of which is dependent on global charging of the surfaces.